The Effects of Local Ionospheric Decorrelation on LAAS: Theory and Experimental Results

Jock R. I. Christie, Ping-Ya Ko[§], Andrew Hansen, Donghai Dai, Samuel Pullen, Boris S. Pervan[†], Bradford W. Parkinson

Department of Aeronautics and Astronautics, Stanford University

[§]*Chung Shan Institute of Technology and Science*

[†]*Illinois Institute of Technology*

Abstract

Solar cycle 23 is expected to reach a maximum in the year 2000. This has produced a recent flurry of research about the possible adverse effects of the ionosphere on the millions of GPS users. The introduction of the Global Positioning System (GPS) ushered in a new era of affordable precise navigation. Differential GPS (DGPS) corrections have reduced positioning errors from about 100 meters to roughly 1 meter, which has led to their proposed use in aircraft precision approach. However, the accuracy of differential corrections is somewhat limited by spatial and temporal decorrelation of the atmosphere. Much of the recent increase in GPS usage, as well as the development of precision landing requirements were developed near solar minimum. Although consideration was made for increased levels of sunspot and ionospheric activity, it is prudent to better characterize ionospheric decorrelation. This paper will present both theoretical and experimental results in this regard.

Currently assumed value of spatial decorrelation for the ionosphere is about 2 mm/km, which is equivalent to an error of only 3 centimeters error due to the ionosphere at 15 kilometers from the DGPS reference station. However, this value is based on relatively smooth models of the ionosphere. This value seems overly optimistic when compared to a documented ionospheric gradient of 55 mm/km, which is certainly too conservative.

Much of the development of the prototype landing systems has occurred in the last three or four years, close to the solar minimum. Current requirements for precision landing, which limit integrity risk to one undetected navigation hazard in a billion trials, suggest that we must fully characterize ionospheric decorrelation. This paper seeks to obtain statistical bounds for the ionospheric decorrelation effects on a LAAS architecture.

Archived data from the National Satellite Test Bed (NSTB = WAAS Prototype) was analyzed to characterize the spatial gradients. The impact of filter time constants on pseudorange error was calculated. This delay artifact of the CSC architecture was examined to ensure integrity.

This paper seeks to obtain statistical bounds for the ionospheric decorrelation effects on a LAAS architecture.

Introduction

Measurement decorrelation is an issue for precision DGPS applications such as LAAS. The rate of decorrelation determines the inter-station spacing for WAAS. Decorrelation is roughly linear with range from the reference station, increasing as you move farther from the reference station. This increase in error does not necessarily lead to a reduction in safety, since the aircraft is typically higher above local terrain when it is further from the airport. Previous GPS research in Antarctica measured a decorrelation of 50 cm over a 9 km baseline, all of which was attributed to the ionosphere [Goad]. This gradient of 55 mm/km, is 20 times larger than the typical quoted values. While polar regions typically experience larger values of TEC, this single observation is alarming since it is certainly not the worst possible value, just the worst value observed during the short campaign.

Ionospheric gradients (decorrelation) can be visualized in *Figure 1*. As the distance between the reference station and the mobile user increases, the lines of sight will travel through different parts of the ionosphere.

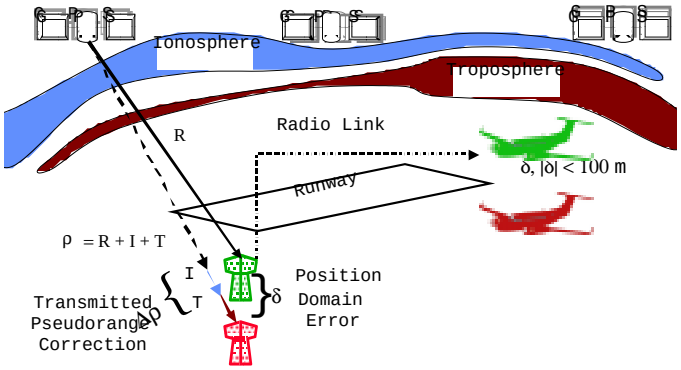

Figure 1 LAAS Overview

For a single frequency receiver, there are two observables, the *pseudorange* (ρ) and the *carrier phase* (ϕ). Both of

ION NTM-99: Atmospheric Effects San Diego, California January 1999
Contact: Jock Christie, HEPL-GPS, Via Palou, Stanford University, Stanford CA 94305-4085
email) jockc@relgyro.stanford.edu Phone) 650.723.9349 Fax) 650.725.9167

these are the sum of the true range (R) and various error terms; including the Ionosphere (I), the Troposphere (T) and the integer ambiguity (Nλ), clock error terms (B-b^k); as well as measurement noise(ν).

1) $$\rho = R + I + T + (B - b^k) + \nu_{code}$$
$$\phi = R - I + T + N\lambda + \nu_{carrier}$$

While the true range to the satellite is not known, a very good estimate can be made based on the satellites' broadcasted position and the reference receiver's known position. Local DGPS installations typically transmit just *scalar* pseudorange correction terms (Δρ). Such systems do *not* transmit the position error.

2) $$\hat{R}_{ref} = |\hat{x}_{\text{sat broadcast}} - \hat{x}_{\text{ref known}}|$$
$$\Delta\rho = \rho_{ref} - \hat{R}_{ref} \cong \delta R + I + T + (B - b^k) + \nu_{code}$$

When the pseudorange correction (Δρ) is received by the mobile user, it is subratcted from the measured pseudorange. This improved estimate of the actual range from the mobile user to the satellite allows the user to better estimate their position. Obviously measurement noise will affect the accuracy of the transmitted correction. However, filtering should remove any zero mean measurement errors. Of greater concern are biases that may be introduced because the user and the reference receiver measure pseudoranges through different portions of the ionosphere.

3) $$\hat{R}_{ac} = \rho_{ac} - \Delta\rho$$

Carrier measurement noise is substantially less than code measurement noise. Carrier smoothed code (CSC) is used to improve the noise characteristics of the pseudorange correction (Δρ).

The rate at which the pseudorange correction changes determines the interval for transmitting corrections. Slower errors require less frequent corrections for the same total error. Conversely, as specified for LAAS, the same update rate with slower errors will improve the positioning accuracy.

$$\frac{d}{dt}\Delta\rho \cong \frac{d}{dt}\delta R + \frac{dI}{dt} + \frac{dT}{dt} - \frac{db^k}{dt}$$

4) $$\widehat{I} = 0.5(\rho - \phi) = I - 0.5N\lambda$$

$$\frac{d}{dt}\widehat{I} = 0.5\left(\frac{d\rho}{dt} - \frac{d\phi}{dt}\right)$$

It is interesting to consider which error terms change most quickly. *Table 1* shows estimated decorrelation velocities for various error terms. It is well known that Selective Availability (SA) dominates the error rate. In fact, the typical SA velocity is about 10x faster than the velocity of the next fastest error source.

	Velocity (mm/s)	Acceleration (mm/s^2)	Spatial (mm/km)
S/A (clock errors)	210	4	~0
Ionosphere	20	~0	2
Ephemeris	10	1	5
Troposphere	~0	~0	2

Table 1: Decorrelation Terms for the GPS Signal in Space
Excerpted from [GPS, vol II], p. 25

Differential ionosphere delay is the path length difference between the ground reference station (the Ground) and the aircraft (the Air) when the satellite signal penetrates the ionosphere. This differential delay is clearly illustrated in *Figure 2* This error source has previously been ignored by

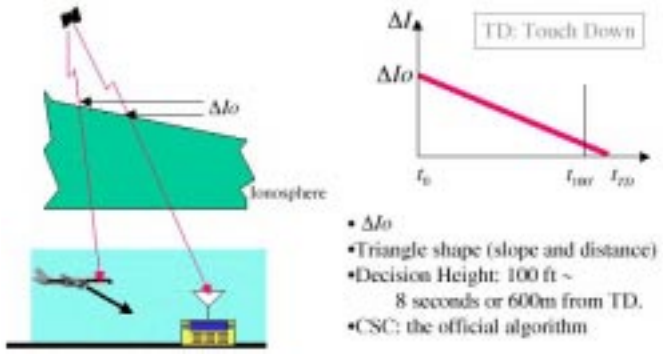

Figure 2 Ionospheric Gradient as observed by reference and mobile GPS users.

assuming that the ionosphere spatial decorrelation for LAAS users is negligible due to the fact that the Air and the Ground are physically close to each other. However, the effect of the officially selected Carrier Smoothed Code (CSC) on the differential ionosphere delay has not yet been extensively studied. The purpose of this work is to better understand the ionospheric gradients, and to examine the effect of the differential carrier smoothed ionosphere delay on LAAS.

The Initial Approach Fix is made at roughly 54 km (30 nautical miles), which corresponds to t_0 in the right half of *Figure 2*. The difference in the ionosphere is essentially the gradient times the distance between the aircraft and the airport. As the airplane approaches the runway, the spatial decorrelation of the ionosphere decreases. At touchdwon the differential ionosphere delay is zero.

LAAS uses carrier smoothed code (CSC) independently at the ground and the air receivers. The air receives the CSC pseudorange correction from the ground and subtracts it from the air's carrier smoothed pseudorange for positioning. Therefore, the differential ionosphere effect has transformed into a differential carrier smoothed ionosphere delay.

Previous Work

Previous research has examined ionospheric decorrelation for the local area Differential GPS (DGPS), but none of them discussed the differential carrier smoothed ionosphere delay. *Goad[1990]* observed 0.5m slant differential ionosphere error over 9km baseline in antarctica during the last solar maximum period. *Wanninger[1993]* recorded a 5m gradient of the ionosphere over a 100km baseline in Brazil during the last solar maximum period. *Warnant[1997]* discussed the potential impact of Travelling Ionospheric Disturbances (TID) and the resulting severe ionosphere gradient over a 15 to 20km baseline, and the limitations for geodetic applications of DGPS. *Doherty[1997]* reported a 12 mm/sec temporal vertical ionosphere gradient in the evening at Fairbanks, AK., in a solar moderate period. These observed ionosphere gradients are useful reference for the study of the differential carrier smoothed ionosphere delay.

Differential Carrier Smoothed Ionosphere Delay

The observed ionosphere is constantly changing. As shown in *Equation 5*, the rate of change is the sum of a temporal term and a spatial term. The first term is the temporal term and is the result of changes in the overall shape of the ionosphere. The spatial term is due to the rapid motion of the Ionosphere Pierce Point (IPP)

$$5) \quad \frac{DI}{Dt} = \underbrace{\frac{\partial I}{\partial t}} + \underbrace{\frac{\partial I}{\partial x_{IPP}}\frac{\partial x_{IPP}}{\partial t} + \frac{\partial I}{\partial y_{IPP}}\frac{\partial y_{IPP}}{\partial t} + \frac{\partial I}{\partial z_{IPP}}\frac{\partial z_{IPP}}{\partial t}}$$

An analytical expression of the differential carrier smoothed ionosphere delay was previously derived [Christie, Ko] as shown in *Equation 6*

$$6) \quad \Delta I_{\text{slant}}(t,x) = I_{\hat{a}} - I_g \approx Ob\left\{\left[2(\tau_a - \tau_g)\frac{\partial I_v}{\partial t}\right|_t\right] + \frac{\partial x_{IPP}}{\partial x}[x + 2(\tau_a - T_s)v]\frac{\partial I_v}{\partial x_{IPP}}\Big|_t\Bigg\}$$

The ionosphere is a complex function of time and pierce point location (x_{IPP}). The resulting difference after filtering is even more complex and depends on filtering time constants in the air (τ_a) and the ground (τ_g), as well as the aircraft velocity (v) and the sampling inteval (T_s)

The first term in *Equation 6* can be eliminated by setting the filter time constants equal. The second term is proportional to the spatial gradient, and can not be readily eliminated, except by setting the air filter time constant (τ_a) slightly larger than the sampling interval (T_s). This is not feasible since $\tau_a \approx 100$ sec, and $T_s \approx 0.5$ sec.

This analytical expression is a very useful tool for the detailed analysis of the effect of the differential carrier smoothed ionosphere delay on the LAAS availability that requires further analysis.

Evaluating *Equation 6*, with x=2 km, v=60m/s, τ_a=100s, then the effective distance is nearly 14 kilometers. Even a smallish gradient of 2 mm/km would produce 28 mm or error in the filter when the aircraft touches down. 28 mm of error is substantial relative to the MASPS requirements detailed in the next section.

The the need for smoothing suggests a longer time constant, whereas the goal of minimizing divergence suggests a short filter time constant.

MASPS Requirements

The RTCA has derived upper bounds for the residual errors due to DGPS for the Signal in Space (SIS). This model is expressed in the following equation:

$$7) \quad \sigma_{res} \le \sqrt{a_2^2 + \left(\frac{a_3}{\sin\theta}\right)^2}$$

The residual error is composed of two distinct types of error source. The a_2 term is independent of elevation angle and contains errors due to SA (clocks), ephemeris, multipath, and receiver noise. The a_3 term is due to the **zenith** delay of the ionosphere and the troposphere. Note that the obliquity correction in *Equation 7* is overly conservative for the ionospheric error at low elevation angles. The following analyses examines only the zenith delay for the ionosphere.

The following table summarizes the specifications for the standard deviation at the decision height (h = 100 feet = 30.5 meters), and at the service ceiling (h = 1290 feet = 363 m)

		σ_{tropo}	σ_{iono}	σ_{total}
Cat I, II	DH = 61 m	20 mm	20 mm	30 mm
	CEIL = 393 m	130 mm	130 mm	185 mm
Cat III	DH = 30.5 m	7 mm	7 mm	10 mm
	CEIL = 393 m	91 mm	91 mm	130 mm

Table 2: MASPS Requirements for Cat I, II, and III

The MASPS specification states that requirements are proportional to the altitude, which results in a tapered "tunnel", much like was present with the ILS specifications.

Inhomogeneities in the ionosphere certainly lead to some spatial decorrelation of the correction. Gradients in the ionosphere will produce a bias between the aircraft and

receiver estimates of the ionosphere. This bias is typically quite small, but the use of CSC magnifies the bias, producing an error roughly equal to the ionospheric error that existed two time constants before.

Ionosphere Model

The ionosphere is often modeled as a thin slab with at a height of 350km above the reference geoid as shown in *Figure 3*. The obliquity factor (Ob) is defined as the ratio of the measured slant delay over the vertical delay. The obliquity is a function of the satellite elevation and the ionospheric shell height, as shown in *Equation 8*. It varies from about 3 at low elevations to 1 near the zenith.

$$8) \quad \mathrm{Ob}(el) = \frac{I_{\mathrm{slant}}}{I_{\mathrm{vertical}}} = \frac{1}{\sqrt{1-\left(\frac{R_e}{R_e+h}\cos(el)\right)^2}}$$

For the differential ionosphere, we are concerned with two things: the distance between the Ionosphere Pierce Points (IPP) of the Ground and the Air as the Δl_{IPP} shown in *Figure 3* and the vertical spatial gradient.

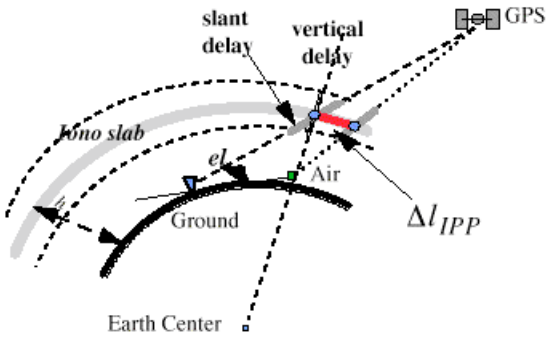

Figure 3 Ionosphere Shell Model

In the 2-D case the IPP distance is a function of the satellite elevation (el) and is proportional to the baseline distance (shown as R0). The unit IPP distance $\Delta l_{IPP,u}$ ranges from 0 when the satellite is at low elevation to almost 1 when the satellite is near the zenith. Generalizing to the 3-D case, $\Delta l_{IPP,u}$ is small when the satellite is roughly in line with the user-reference baseline. $\Delta l_{IPP,u}$ is almost 1 when the satellite is roughly perpendicular to the user-reference baseline

The 2-D differential (slant) ionosphere delay can be derived from *Figure 3*, and is equal to the product of the spatial gradient, the Geometry Factor and the baseline, where the Geometry Factor is defined as $\mathrm{Ob}\Delta l_{IPP,u}$

$$9) \quad \Delta I = I_a - I_g \approx \frac{dI_v}{dl_{IPP}} Ob\Delta l_{IPP,u} R_0$$

IPP Distance & Geometry Factor

The 2-D analysis can be extended into the real (3-D) world. The unit IPP distance ($\Delta l_{IPP,u}$) versus the azimuth and the elevation angles of a satellite is shown below in *Figure 4*.

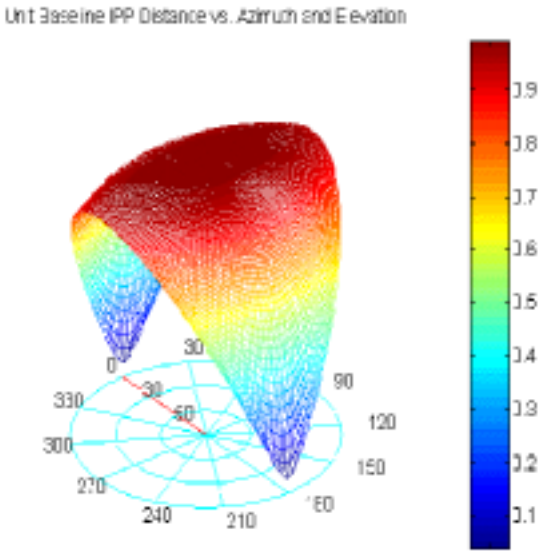

Figure 4 3-D Unit baseline IPP distance
Normalized IPP distance as a function of satellite azimuth and elevation.

When the satellite is along the red baseline (azimuth ~ 0° or 180°), $\Delta l_{IPP,u}$ varies from zero at low elevations, to almost one at the zenith, like the 2-D results. When the satellite is perpendicular to the baseline (azimuth ~ 90° or 270°), the unit IPP distance is almost one for all elevation angles.

The geometry factor as we defined previously is shown in *Figure 5*. The geometry factor represents the sensitivity to spatial gradients in the ionosphere. The geometry factor can be as much as 2.8 for low elevation satellites that are roughly perpendicular to the aircraft-reference baseline.

Approach Geometry

The azimuth from the reference receiver to the mobile user, and the azimuth to the satellite also determine susceptibility

The gradient of the ionosphere, and the position of the mobile user can both be expressed as vectors.

$$10) \quad \frac{\vec{dI}}{dr} = \left[\frac{dI}{dE}\ \frac{dI}{dN}\right] = \left|\frac{dI}{dr}\right|\left[\sin\theta_I\ \cos\theta_I\right]$$

$$11) \quad \vec{R} = |R|\left[\sin\theta_A\ \cos\theta_A\right]$$

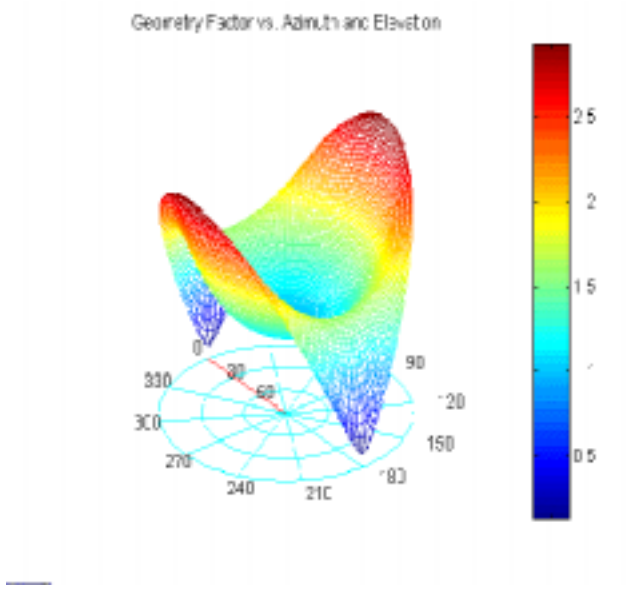

Figure 5 **3-D Geometry Factor**
Geometry factor ($Ob\Delta l_{IPP,u}$) as a function of satellite azimuth and elevation.

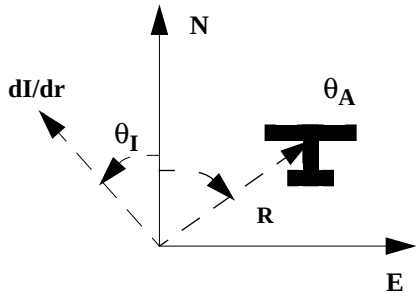

Figure 6 **Aircraft Approach Geometry**

These two vector quantities can be combined to determine the effective difference in the ionosphere that would be observed by the aircraft.

$$\Delta I = \frac{\overrightarrow{dI}}{dr} \bullet \hat{R} = \left|\frac{dI}{dr}\right| |R| \cos(\theta_I - \theta_A) \quad 12)$$

Equation 12 makes intuitive sense in that a large gradient perpendicular to baseline from reference receiver to mobile user will have negligible effect.

The previous section of this paper discussed the effect of satellite geometry without considering the direction of the gradient. Multiplying*Figure 5* by the magnitude of the ionospheic gradient and the cosine of the direction of the gradient. The worst case occurs when the gradient is parallel to the baseline. In that case, if a low elevation satellite is perpendicular to the baseline, then the differential carrier smoothed ionosphere delay will be 2.8 times the ionosphere gradient times the baseline.

For an ionospheric gradient of 0.05m/km [Wanninger], and a 15 km baseline, the differential carrier smoothed ionosphere delay could be 2.1 meters in the range domain. This result is based on a carrier smoothing time constant $T_s \approx 100$ s. Use of a longer time constant in LAAS community, will lead to a more severe differential ionosphere delay. The magnitude of this differential carrier smoothed ionosphere delay can be larger than that of the carrier smoothed multipath error of about 10 to 15 centimeters.

Ionospheric Gradient from WAAS Data

Various Wide Area Augmentation Systems (WAAS) are in development on several continents, namely in Japan, North America, and in Europe. As shown in , the North American WAAS uses more than two dozen monitor stations, primarily in the Continental United States (CONUS) to observe all satellites in view. These measurements are combined in a central location, to generate *vector* corrections of the satellite observations.

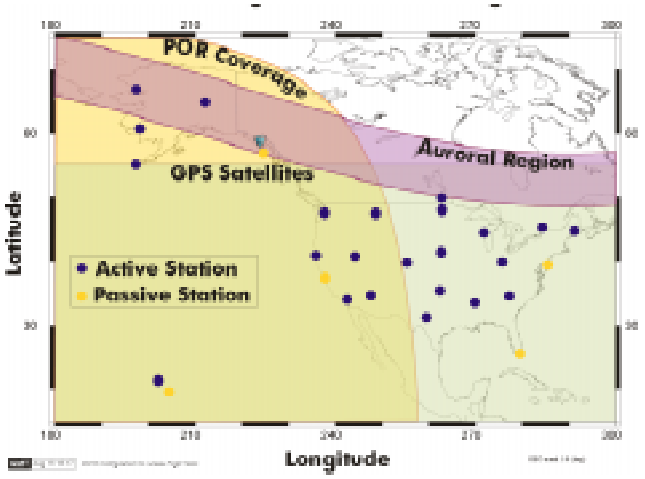

Figure 7 **WAAS reference station in the United States**
Note only three of the NSTB stations are in the auroral region.

At the core of WAAS, the observations are used to determine the local ionospheric conditions at each monitor station, then this data is fit to a grid placed. The user interpolates between grid points to calculate the local vertical ionospheric value. An alternative modelling technique [Hansen] uses spherical harmonics, eliminating the need for a grid. Spherical harmonics are associated Legendre polynomials of degree n and order m, and are a function of the user's longitude(λ) and colatitude (Θ), as expressed in the solar-magnetic frame.

$$I_v(\Theta, \lambda) = \sum_{n=0}^{N_{max}} \sum_{m=0}^{n} [C_{nm}\cos(m\lambda) + S_{nm}\sin(m\lambda)] P_{nm}\cos(\Theta) \quad 13)$$

The associated Legendre Polynomials are defined as follows

14) $$P_n^m(x = \cos\theta) = (1 - x^2)^{\frac{m}{2}} \cdot \frac{d^m}{dx^m} P_n(x)$$

The WAAS vertical ionospheric delay given in *Equation 13* can be easily differentiated with respect to the longitude (λ), This gradient is then converted from radians of longitude to kilometers, where E denotes East.

15) $$\frac{\partial}{\partial E} I_v(\Theta, \lambda) = \frac{1}{R_e \cos\left(\frac{\pi}{2} - \Theta\right)} \sum_{n=0}^{N_{max}} \sum_{m=0}^{n} [S_{nm}\cos(m\lambda) - C_{nm}\sin(m\lambda)] m P_{nm}\cos(\Theta)$$

Similarly, the gradient in the North-South direction requires taking the derivation of the Legendre polynomial, with respect to the colatitude (Θ).

16) $$\frac{\partial}{\partial N} I_v(\Theta, \lambda) = \frac{-1}{R_e} \sum_{n=0}^{N_{max}} \sum_{m=0}^{n} [C_{nm}\cos(m\lambda) + S_{nm}\sin(m\lambda)] \left\{ \frac{m \cdot \cos\Theta}{\sin\Theta} \cdot P_n^m(\cos\Theta) - P_n^{m+1}(\cos\Theta) \right\}$$

Unfortunately, this expression approaches a singularity in polar regions, as $\sin(\theta = k\pi) \Rightarrow 0$, where the largest ionospheric gradients are presumably found.

WAAS is capable of generating valid coefficients up to about degree n=15, before measurement noise dominates. These coefficients can be used in *Equation 15* and *Equation 16* to calculate the local spatial gradient of the ionosphere.

One limitation of any WAAS implementation is that data is collected only from a very small portion of the Earth's surface. The continental United States (conus) covers approximately 4.7% of the globe, and all 50 states together cover approximately 5.6% of the globe. Thus all the data is concentrated in a small region and it is dangerous to extend a WAAS solution that covers CONUS to any other region.

Large ionospheric gradients are not typically found at temperate latitudes. The larger gradients are more likely to occur near the equator or in the auroral region. Unfortunately, there are not enough observations available from the Alaskan portion of the NSTB to permit tomographic estimation of the ionosphere over Alaska.

Figure 8 shows contour intervals of the vertical ionosphere derived from WAAS data for a single epoch. As expected, the vertical ionosphere is larger at lower latitudes.

Figure 9. shows contour intervals of the magnitude of the spatial gradient of the vertical ionosphere. The larger gradients occur at lower latitudes for this particular data set.

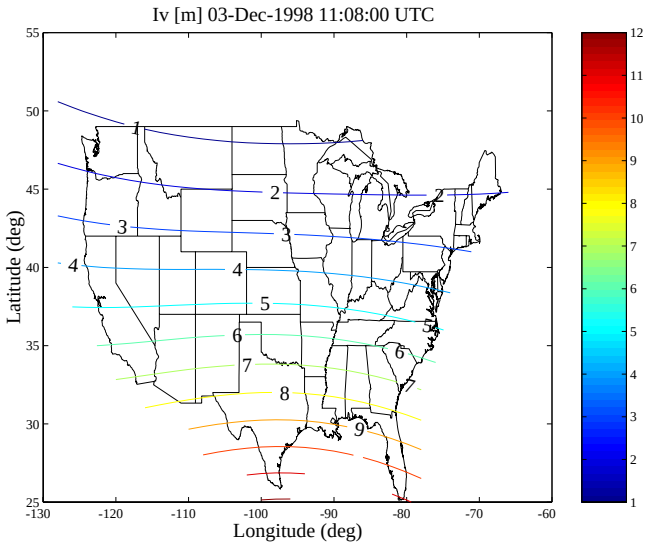

Figure 8 Contour Map of Vertical Ionosphere over Conus

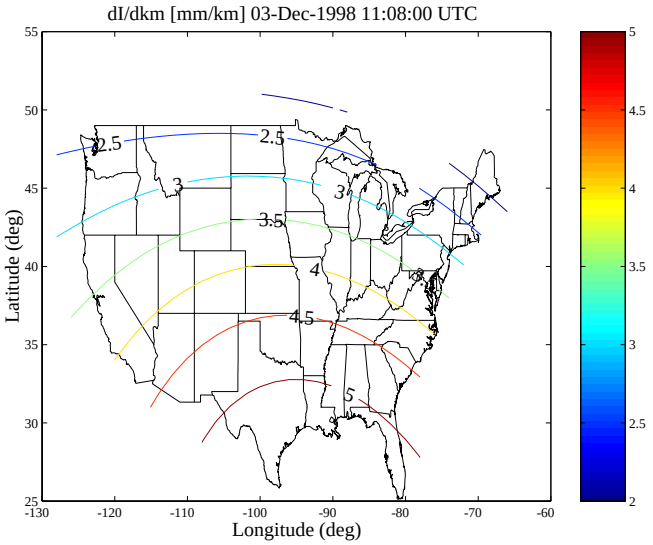

Figure 9 Gradient of vertical Ionosphere over Conus

A contour interval plot of the temporal gradient is shown in *Figure 10.* This limited data set produced relatively benign levels of ionospheric velocity.

Ionospheric velocities from WAAS

Archived data was used to examine the rate at which the (slant) ionosphere changes at various reference sites. The ensemble over long periods should reflect the underlying distribution of the ionospheric velocities.

At Stanford a filter was implemented in the WAAS testbed to record and monitor the ionospheric velocity based on dual frequency measurements. These observations are resampled every hour to ensure an unbiased estimate of the actual velocities.

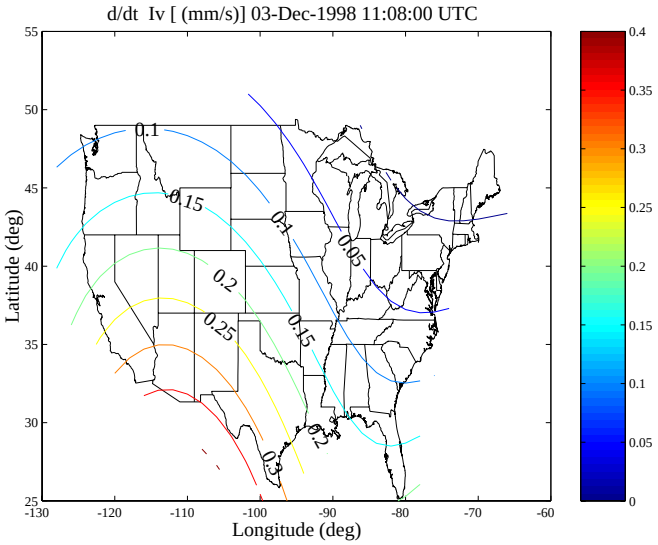

Figure 10 Contour Map of Vertical Ionospheric Velocity.

All sites in the NSTB were examined for calendar year 1998. Data was typically available for more than 190 days of the year. Data was available for most of the sites in the NSTB. However only the values from four sites in Alaska are shown below.

As shown in *Figure 11*, the resulting distributions are

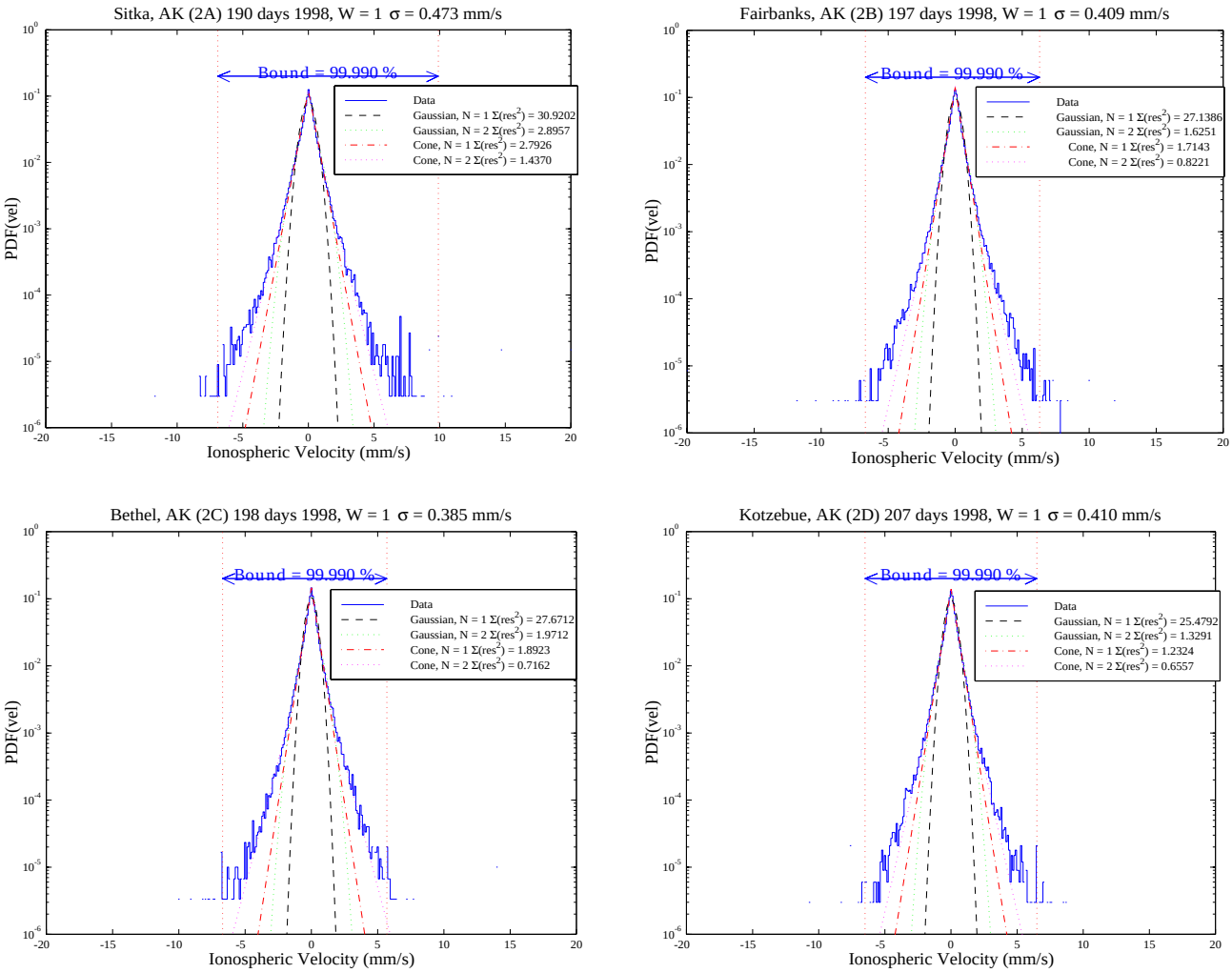

Figure 11 Histograms of Slant Ionospheric Velocities for 4 NSTB sites in Alaska during 1998
The panels show histograms from Sitka, Fairbanks, Bethel, and Kotzebue Alaska.

not gaussian. An algorithm was developed in Matlab to fit multiple gaussians to the histogram in a least squares sense. This alogrithm was supposed to better model the tails of the distribution.

A weighting matrix was used to increase the weight of the tails. Weights were assigned based on the absolute velocity raised to a small integer power (0 1 or 2). These weights were also normalized, so that in each case, the sum of all weights was unity. This weighting method did not work all that well. Even weighting (exponent of 0) ignored the tails, while weighting of 2 caused the solution to chase the tails of the distribution. Non-integer weighting was not explored. All plots were based on a weighting of 1.

An alternative probability distribution was explored that better matches the actual distributions shown above.

$$17) \quad \mathrm{PDF}(x) = \frac{\log 10}{2\alpha} 10^{-\frac{|v|}{\alpha}} = \frac{\log 10}{2\alpha} e^{-(\log 10)\frac{|v|}{\alpha}}$$

For this 'conical' distribution, it is very easy to calculate the probabilites of exceeding a certain limit, as shown in *Equation 18*

$$18) \quad P(|v| \geq k\alpha) = 1 \times 10^{-k}$$

While this distribution is *too conservative*, it is very simple to calculate the probabilites of certain values, as shown in *Table 3* .

k	$P(\|v\| \geq k\alpha)$
6	1×10^{-6}
7	1×10^{-7}
8	1×10^{-8}
9	1×10^{-9}

Table 3: Seleceted probabilities for 'cone' type PDF

Statistics for the slant ionospheric velocities for the five Alaskan sites are shown in *Table 4* Standard deviations (σ) and alphas (α) were calculated.

City	TRS #	# epochs	σ (mm/s)	α (mm/s)
Sitka	2A	1675810	0.4729	0.9465
Fairbanks	2B	1648358	0.4088	0.8173
Bethel	2C	1494743	0.3845	0.7790
Kotzebue	2D	1673962	0.4098	0.8202
Cold Bay	2E	1399107	0.3694	0.7432

Table 4: Observed Standard Deviations of Velocities

The worst case number from *Table 4* of $\alpha = 0.9465$ mm/s, implies that the probablility of the velocity exceeding 10 mm/s is roughly one in a billion. Note that there are occasional epochs visible in the histograms of *Figure 11* that exceed 10 mm/s. Using the standard deviation of s = 0.4729 mm/s suggests a 1 in a billion limit of 2.52 mm/s which is far too optimistic.

Conclusions

Spatial ionospheric gradients ranging from 2 to 5 mm/km were observed using the WAAS tomographic method. Unfortunately, there was not enough data available to develop meaningful statistics in time for this paper.

Because of the filter lag of the carrier smoothed code, it is important to better quantify these gradients.

The ionosphere can produce small decorrelation errors when the aircraft (user) is several kilometers from the DGPS reference station. These errors are fairly small relative to the precision of a code based DGPS system and are therefore essentially negligible. The use of Carrier Smoothed Code can significantly increase the magnitude of the ionospheric error at the touchdown point. The ground and air must use equal time constants in the smoothing algorithm.

However, these same small errors are a large part of the error budget for a carrier phase DGPS. In particular, the divergent nature of the ionosphere leads to erratic results when using carrier smoothed code.

References

[Christie] Christie, Jock R. I., Ping-Ya Ko, Boris S. Pervan, Per K. Enge, J. David Powell, Bradford W. Parkinson, "Analytical and Experimental Observations of Ionospheric and Tropospheric Decorrelation Effects for Differential Satellite Navigation during Precision Approach", ION GPS-98, Nashville, Tennessee, USA, September 1998

[Clynch] Clynch, J., Note to RTCA

[Doherty] Doherty, Patricia H. et al. "Spatial and temporal variations in ionospheric range delay", ION GPS-97, Kansas City, MO, USA., September 1997

[Fuller] Fuller, Richard A., Todd Walter, Sharon Houck, Per Enge, "Flight Trials of a Geostationary Satellite Based Augmentation System at High Latitudes and Dual Satellite Coverage", Presented at ION National Technical Meeting 1999, San Diego, CA, January 1999

[GPS] Global Positioning System, Theory and Applications, edited by Parkinson and Spilker, AIAA Washington DC

[Goad] Goad, Clyde C., "Optimal filtering of pseudoranges and phases from single-frequency GPS receivers", *Navigation*, Vol. 37, No. 3, Fall 1990

[Gregorius] Gregorius, Thierry, and Geoffrey Blewitt, “The Effect of Weather Fronts on GPS Measurements”, GPS World, May 1998

[Griffith] Griffith, Cheryl, Stephen Peck, Juan Ceva, and Rajendra Malla, "Should WAAS get Ride of the MET Instruments", ION January 1997

[Hansen97] Hansen, Andrew, Todd Walter and Per Enge, “Ionospheric Correction Using Tomography”, ION GPS'97, Kansas City MO, September 1997

[Hansen98] Hansen, Andrew, “Real-time Ionospheric Tomography Using Terrestrial GPS Sensors”, ION GPS’98, Nashville, Tennessee, USA, September 1998

[Pervan] Pervan, Lawrence et. al., "Flight Test Evaluation of an Alternative Local Area Augmentation System Architecture", *Navigation*, Vol. 45, No. 2, Summer 1998

[Rabinowitz] Rabinowitz, Matt, Bradford Parkinson, Clark Cohen, “The Application of LEOS to Cycle Ambiguity Resolution on Navstar Transmissions for Kinematic Carrier-Phase Positioning”, ION GPS’97. Kansas City, Missouri, September 1997.

[Wanninger] Wanninger, Lambert, Gunter Seeber, and Milton A. Campos, 'Limitations of GPS in Central and South America Due to The Ionosphere', presented at the International “Cartography - Geodesy", Conference, Maracaibo, Venezuela, Nov 24 - Dec 4, 1992

[Wanninger] Wanninger, Lambert, "Effects of the Equatorial Ionosphere on GPS." , *GPS World*, July 1993.

[Warnant] Warnant, René, "Influence of the ionospheric refraction on the repeatability of distances computed by GPS", ION GPS-97., Kansas City, MO, USA., September 1997

Acknowledgments

We would like to thank the FAA for their ongoing support of GPS research at Stanford University. Special thanks to all the people, especially Todd Walter, and Per Enge in the Stanford WAAS Lab for generously sharing their data.

Stanford GPS Lab
Stanford, CA 94305-4085

http://www.stanford.edu/group/GPS